Asian Journal of Pharmaceutical Sciences 18 (2023) 100814

Available online at www.sciencedirect.com

ScienceDirect

journal homepage: www.elsevier.com/locate/AJPS

Original Research Paper

KCNJ15 deficiency promotes drug resistance via affecting the function of lysosomes

Xinbo Qiao[a,b,c,1], *Yixiao Zhang*[a,b,c,1], *Zhan Zhang*[a,b,c,1], *Nan Niu*[a,b], *Haonan Li*[d], *Lisha Sun*[a,b,c], *Qingtian Ma*[a,b,c], *Jiawen Bu*[a,b,c], *Jinchi Liu*[a,b,c], *Guanglei Chen*[a,b], *Jinqi Xue*[a,b], *Yongliang Yang*[a,d,*], *Caigang Liu*[a,b,c,*]

[a] *Department of Oncology, Shengjing Hospital of China Medical University, Shenyang 110000, China*
[b] *Cancer Stem Cell and Translational Medicine Laboratory, Shengjing Hospital of China Medical University, Shenyang 110000, China*
[c] *Innovative Cancer Drug Research and Development Engineering Center of Liaoning Province, Shenyang 110000, China*
[d] *School of Bioengineering, Dalian University of Technology, Dalian 116000, China*

ARTICLE INFO

Article history:
Received 4 November 2022
Revised 19 March 2023
Accepted 22 April 2023
Available online 12 May 2023

Keywords:
Breast cancer
Cancer progression
Drug resistance
Lysosome
KCNJ15

ABSTRACT

The altered lysosomal function can induce drug redistribution which leads to drug resistance and poor prognosis for cancer patients. V-ATPase, an ATP-driven proton pump positioned at lysosomal surfaces, is responsible for maintaining the stability of lysosome. Herein, we reported that the potassium voltage-gated channel subfamily J member 15 (KCNJ15) protein, which may bind to V-ATPase, can regulate the function of lysosome. The deficiency of KCNJ15 protein in breast cancer cells led to drug aggregation as well as reduction of drug efficacy. The application of the V-ATPase inhibitor could inhibit the binding between KCNJ15 and V-ATPase, contributing to the amelioration of drug resistance. Clinical data analysis revealed that KCNJ15 deficiency was associated with higher histological grading, advanced stages, more metastases of lymph nodes, and shorter disease free survival of patients with breast cancer. KCNJ15 expression level is positively correlated with a high response rate after receiving neoadjuvant chemotherapy. Moreover, we revealed that the small molecule drug CMA/BAF can reverse drug resistance by disrupting the interaction between KCNJ15 and lysosomes. In conclusion, KCNJ15 could be identified as an underlying indicator for drug resistance and survival of breast cancer, which might guide the choice of therapeutic strategies.

* Corresponding authors at: Department of Oncology, Shengjing Hospital of China Medical University, Shenyang 110000, China.
E-mail addresses: everybright99@foxmail.com (Y. Yang), liucg@sj-hospital.org (C. Liu).
[1] These authors contributed equally to this work.
Peer review under responsibility of Shenyang Pharmaceutical University.

https://doi.org/10.1016/j.ajps.2023.100814

1. Introduction

Drug resistance-induced cancer progression represents as a main challenge for cancer treatment. Patients who develop multidrug resistance after receiving treatments typically pose significantly shortened disease-free survival (DFS). In 2022, more than 600,000 cancer deaths are projected to occur due to primary or acquired therapeutic resistance in the United States alone. Therefore, the investigation on the mechanisms of drug resistance could improve the therapeutic effectiveness and patient prognosis.

In the clinical practice, due to the lack of effective therapeutic strategies, it will be a fatal blow to breast cancer patients when drug resistance occurs, especially for triple-negative breast cancer (TNBC) patients who mainly rely on chemotherapy. The process of developing drug resistance in tumors is extremely complicated during which the potential mechanisms such as gene mutations, formation of immunosuppressive tumor microenvironment, changes of signaling pathways and epigenetic alterations have been proposed [1–4]. However, most mechanisms can only explain the phenomenon of resistance to a single or several drugs. In addition to these genetic mechanisms, mounting evidences reveal the importance of non-mutational changes in therapeutic evasion [5–8]. Therefore, exploring the underlying mechanisms and solutions of tumor drug resistance is urgently needed [9,10].

Lysosome, an organelle filled with various acidic hydrolases, is mainly responsible for the degradation of proteins, nucleic acids, polysaccharides and other biological macromolecules [11,12]. Compared to the neutral microenvironment of cytoplasm (pH is about 7.2), lysosomes exhibit their maximal enzymatic activity at a relatively low pH (≤ 5) [13]. On the surfaces of lysosomes, v-ATPase, a multi-subunit complex and proton pump, transports protons into the lysosomal lumen to maintain the low pH [14]. V-ATPase contains 8 V1 domains (A–H) for ATP hydrolysis and 5 membrane-spanning V0 domains (a, c, c', d, e and ATP6AP1) [15–17]. Growing attention has been drawn into the effects of V-ATPase in increasing the metastatic potential and survival of cancer cells in acidic tumor environment [18–20]. However, the underlying mechanisms of how lysosomes regulate drug metabolism in tumor cells remain unclear.

Potassium voltage-gated channel subfamily J member 15 (KCNJ15) protein, a type of inward rectifying potassium ion channel, is widely distributed among various tissues to maintain the resting potential of cell membrane [21,22]. KCNJ15 protein has been shown to participate in the tumor proliferation, senescence, invasion, and metastasis [23,24]. However, the relationship between KCNJ15 protein and lysosomes, as well as their interactions in tumor drug resistance remains unclear.

Here, we first report that KCNJ15 is essential to maintain the function as well as stability of lysosomes in breast cancer cells. Low KCNJ15 expression in breast tumors were observed to interact with the subunits of V-ATPase which serves as an ATP-driven proton pump positioned at lysosomal surfaces, thereby leading to the dysfunction of lysosomes and drug resistance. In addition, upregulation of KCNJ15 protein can subsequently decrease lysosome quantity, inhibit the cell proliferation, induce the apoptosis of tumor cells, and enhance the cell sensitivity to therapeutic drugs. To explore the clinical significance of this study, breast cancer tissues were collected from patients and analyzed. Our results indicated that KCNJ15 expression was lower in neoadjuvant chemoresistant tumors compared with chemosensitive tumors, which is significantly related to poorer DFS of patients. These findings suggested that the expression status of KCNJ15 might act as an underlying indicator for the drug resistance and chemotherapy efficacy of breast cancer, which may provide insights to the choice of strategies for cancer treatment.

2. Materials and methods

2.1. Cell culture

The MDA-MB-231, SKBR3 and MCF-7 human breast cancer cells were all obtained from the American Type Culture Collection (Manassas, VA). In addition, it could be found that the MDA-MB-231 was cultured within the L15 medium of the Leibovitz (Thermofisher, Carlsbad, CA) that was added with the 10% fetal bovine serum (Cellmax, Lanzhou, China), penicillin (100 U/ml) and streptomycin (100 μg/ml) without CO_2 at 37 °C within the humidified incubators. At the same time, MCF-7 and SKBR3 were both cultured within Leibovitz's DMEM medium (Thermofisher, Carlsbad, CA) that was added with the 10% fetal bovine serum, penicillin (100 U/ml) and streptomycin (100 μg/ml) with 5% CO_2 at 37 °C within the humidified incubators.

2.2. Digital phase-contrast microscopy

The PerkinElmer Operetta® was employed to image the individual wells on assay plates. The plates were removed from the incubation, and before being returned to incubation in case of need, per well was imaged through the use of both the brightfield and the phase-contrast microscopy (total area imaged 1.7 mm^2; <20 min/plate). The brightfield images were taken from the bottom 1 μm of per well, and the exposure was 100 ms. In addition, the exposure time of the digital phase-contrast images was 40 ms, which ranged from −5 μm to 5 μm, and the speckle scale was 10 μm.

2.3. Drug sensitivity test

The *in vitro* sensitivity of fresh KCNJ15 positive and negative primary tumor cells to CDK4/6 inhibitor was evaluated through the use of the collagen gel droplet-embedded drug sensitivity test (CD-DST). To be brief, a portion of all the tumor specimens was thinly sliced after being excised. After the treatment with the dispersion enzyme cocktail EZ (Kurabo Industries, Osaka, Japan), it is found that the cell suspension was incubated with KCNJ15 antibody (Cat. # 45738-OTI4F9, Novus, USA) for 30 min, and then was washed with the BSA buffer (Cat. # 130-091-376, Miltenyi, Germany), and was next incubated with the Anti-mouse IgG1-microbeads (Cat. # 130-047-102, Miltenyi, Germany) for 30 min in the

refrigerator (2–8 °C). Following washing and resuspension with BSA buffer, the cells were separated with MS columns (Cat. # 130-041-301, Miltenyi, Germany) by using the MiniMACS separator following the manufacturer's instructions. Next, both of the KCNJ15 positive and negative primary tumor cells were transferred respectively to the collagen-coated flasks (CG-flask, Kurabo Industries) and were cultured within the preculture medium that contained 10% fetal bovine serum at 37 °C overnight in 5% CO_2. In order to get viable cancer cells, the collagen gel was digested through the application of 0.05% collagenase (type I; Sigma-Aldrich Japan, Tokyo, Japan).

2.4. A mouse model of xenograft tumor assays

In accordance with the Guidelines of the Care and Use of Laboratory Animals issued by the Chinese Council on Animal Research, the experimental protocol was reviewed and approved by Shengjing Hospital of China Medical University (2018PS304K). The Human Silaikejingda Laboratory Animals (Changsha, China) provided the female BALB/c nude mice (6 weeks), which were housed within the special pathogen-free facility that can freely obtain both food and water. The tumor growth and body weights of the mice underwent monitoring until the post-cancer cell inoculation for a total of 21 d. When the experiment ended, there was dissection and weighing of the subcutaneous tumors.

2.5. Transmission electron microscopy

Transmission electron microscopy (TEM) was used to examine the ultrastructure of MDA-MB-231/NC and MDA-MB-231/OE KCNJ15 cells. To be brief, the cell groups were collected, fixed within 2.5% glutaraldehyde and embedded. Before being mounted upon the copper grid, the ultra-thin sections (70 nm) were made through the use of a microtome. The sections were stained with the Reynolds lead citrate (2 min) after they were stained with the 4% aqueous uranyl acetate (10 min). In addition, a transmission electron microscope (JEM2000EX, JEOL, Sagamihara, Japan) was used to photoimage the cells.

2.6. Immunofluorescence staining and IHC

Fugene6 was used to transiently transfect the cells with the plasmids. The cells that grow upon the glass coverslips were fixed for 10 min in 4% PFA at 4 °C after they were washed. When finishing the blocking in PBS with 5% goat serum, the suitable antibodies were dealt with in terms of the immunostaining cells.

4% formaldehyde was used to fix the breast cancer specimens, primary and metastatic breast cancer specimens, fresh non-cancer specimens, and fresh breast cancer tissues. Next, all of them were embedded within paraffin and were sliced into sections with 5 μm. From the perspective of the xenograft staining, 10% formalin was used to fix the collected samples. When the paraffin embedding treatment came to the end, the sectioned samples were immunostained in accordance with the standard protocols. ImageJ was used to analyze the cellular co-localization quantification. Table S1(in Supplementary materials) shows the antibodies' information.

2.7. Immunoprecipitation and immunoblotting

The whole-cell lysates of mammalian cells were made through the use of the NP-40 lysis buffer (0.5% NP-40, 1 mM phenylmethylsulfonyl fluoride, 1.5 mM MgCl2, 12.7 mM benzamidine HCl, 10% glycerol, 25 mM HEPES, 0.2 mM aprotinin, 150 mM KCl, 0.5 mM leupeptin and 0.1 mM pepstatin A) at 4 °C for 20 min. That was followed by centrifugation (13,148 g for 10 min). In addition, the supernatants were denatured within 5× SDS sample buffer (8% SDS, 40% glycerol, 200 mM dithiothreitol, 200 mM Tris-HCl pH 6.8 and 0.08% bromophenol blue) for 5 min at 95 °C, and that was followed by SDS–PAGE. Taking into account the immunoblot blocking and antibody incubation, both the 0.1% non-fat dry milk within Tris-buffered saline and the Tween20 (125 mM NaCl, 25 mM Tris-HCl pH 8.0, and 0.5% Tween-20) was adopted. The horseradish peroxidase-conjugated secondary antibodies were detected by using the SuperSignal West Pico (Thermo; 34,087) and Femto (Thermo; 34,095) reagents. As for the immunoprecipitation, the cell lysates were incubated for 2 h with 20 μl magnetic beads (Sigma; M8823). Next, the immunoprecipitates were washed by using the cell lysis buffer three times, eluted through the use of an SDS sample buffer and explored via immunoblotting.

2.8. Protein modeling and protein-protein docking

2.8.1. Protein modeling

The core region (Y78-S177) of KCNJ15 NMR structure (Protein Data Bank [PDB] code: 2K8P) was selected as the template to build the structure using Modeller 9.22 with 1000 decoys. The results were evaluated using DOPE, Molpdf score, DFIRE2, and Procheck, followed by 20 ns molecular dynamics (MD) relaxation. The E1 and E2 domains structure (D20-H631) of LRP5 from Alphafold2 was used for the following research with 20 ns MD optimization and relaxation.

2.8.2. Protein-protein docking

The Zdock program performs a fast Fourier transform searching for all possible binding modes based on shape complementarity, desolvation energy, and electrostatics. In this study, we used Zdock to perform rigid-body docking for KCNJ15 with ATP6V0A1, with some key residues as the preferred during the docking process. The structure of KCNJ15-ATP6V0A1 (PDB code: 6L6R) was taken as the template to filter the complex structure. The most similar complex of KCNJ15 and ATP6V0A1 was used for the following research with 100 ns MD optimization and relaxation.

2.9. Gene expression analysis

RNAs were extracted through the use of the TRIzol (Cat. # T9108, TaKaRa, Japan), and were then reversed-transcribed through the use of the cDNA synthesis kit (Cat. # RR047A, TaKaRa, Japan) in accordance with the protocol for the manufacturers. The experiment was carried out by using the SYBR Green PCR Master Mix (Cat. # RR820A,

TaKaRa, Japan) and the suitable primers (KCNJ15 primer: Fwd 5′- TCAGATGAATTCCGCCATGGATGCCATTC; Rev 5′-GCCTCGAGCCTCAGACATTGCTCTGTT) upon the Fast-Real-Time PCR System. The thermocycling schedule was 95 °C for 30 s, which was followed by the 40 cycles of 95 °C for 3 s and 60 °C for 30 s separately. What is more, the 2-ΔΔCt method was used to calculate the relative mRNA level.

2.10. TCGA analysis

UALCAN is considered to be an interactive web portal for the exploration of The Cancer Genome Atlas (TCGA) gene expression data. It was also employed to investigate the KCNJ15 mRNA expression within normal breast tissue and breast cancer and the survival among a variety of breast cancer subtypes. KCNJ15 relationship with the key regulators in the EMT pathway was carried out within the GEPIA. In addition, the TIMER database shows the relationship between the KCNJ15 and the integrin family within a range of TCGA-BRCA dataset types.

2.11. RNA-sequencing

RNA was isolated from 231-DR2 or no treatment. Before harvesting, the resistant cells were cultured for a week with no drug. The RNeasy Plus Mini Kit was used to harvest the RNA from 3 replicate 10 cm plates for all of the cells (Qiagen 74136). Before the mRNA library preparation, the Agilent Bioanalyzer was used to assess the samples. The libraries were made following the Illumina protocols by the Yale Stem Cell Center Genomics and Bioinformatics Core, and were operated upon the Illumina HiSeq2000. As mentioned before, bioinformatic analyses were carried out. In other words, Bowtie2 was used to map the reads to the human genome (hg38), DESeq2 was used to decide differential gene expression, and pathway analysis used the Gene Set Enrichment Analysis (GSEA) software (34). What is more, the RNA-seq data were stored within the National Center for Biotechnology Information (NCBI) Gene Expression Omnibus database with the accession number being GSE121105.

2.12. Survival analysis of hub genes

With 18,674 cancer samples in total, the influence of the 54,675 genes on survival can be evaluated by using the Kaplan–Meier plotter (http://kmplot.com/analysis/). It includes a total of 5143 breast cancer patients that have relapse-free and overall survival information, majorly in accordance with the GEO, TCGA and EGA databases. This tool can be used to carry out the meta-analysis following the biomarker assessment to contribute to clinical decisions, resource allocation and health care policies. The research used the Kaplan–Meier plotter in breast cancer to explore the survival of individual hub genes. The patients involved two groups following the median of all the hub gene expressions within the Kaplan–Meier plotter for overall survival. By carrying out that kind of classification method, the differences in survival probability between the low-expression group and the high-expression group can be presented.

2.13. Bioinformatics

DEGs were explored by using gene ontology (GO) and the Database for Annotation, Visualization and Integrated Discovery software. Beside, the Kyoto Encyclopedia of Genes and Genomes (KEGG) annotations were used to explore the potential pathways the DEGs included.

2.14. Transduction

In order to set up the MDA-MB-231/NC and MDA-MB-231/OE KCNJ15 cells with the stable overexpression of the KCNJ15 expression, the MDA-MB-231 cells were transduced through the use of the lentivirus (at the infection multiplicity of 10) that included the control shRNA (NC) or the KCNJ15-specific shRNA. Moreover, they were cultured within the 5 μg/ml puromycin for 4 d in order to carry out the selection.

2.15. siRNA and cell transfection

Both the yes-associated protein KCNJ15-specific siRNA (5′-CAUACUUGGAGAGAGAGCUAATT-3′) and the negative control siRNA (5′-UUCUCCGAACGUGUCACGUTT-3′) were obtained through the use of the GenePharma (Shanghai, China), and were adopted to the knockdown expression of the corresponding genes. The CD44-/CD24- MDA-MB-231 cells were cultured at a density of 5×10^5 cells/well within 6-well plates overnight, till there was 70% confluency in case of that they were transiently transfected with the negative control siRNA or KCNJ15-specific siRNA through the use of the Mission siRNA transfection reagents (Sigma-Aldrich, St. Louis, MO, USA) for 2 d. The western blot analysis was used to assess the silencing efficacy for all of the specific genes.

2.16. Cell proliferation assay

To be brief, the MCF-7, MDA-MB-231 and SKBR3 cells expressing KCNJ15 silencing or control shRNA (1×10^3 cells/well), as well as the KCNJ15 knockout MDA-MB-231 cells were cultured within the 96-well plates for either 1 d or 2 d. Cells were exposed to 20 μl freshly prepared 3-(4,5-dimethylthiazol-2-yl)-5-(3-carboxymethoxyphenyl)-2-(4-sulfophenyl)-2Htetrazolium/phenazine ethosulfate (MTS/PES) solution for 4 h. A microplate reader (Bio-Rad, Hercules, CA) was used to measure the absorbance at 490 nm.

2.17. Flow cytometry

The cell cycle analysis kit (C1052, Beyotime, China) was adopted. The transfected cells were seeded at 1×10^5 cells/well in 6-well plates (Corning, NY, USA) for 3 d, harvested using the trypsin method, and fixed at −20 °C within 70% cold ethanol overnight.

2.18. Patients and tissue specimens

171 patients with TNBC in total were selected at the Shengjing Hospital of China Medical University. Following the histological examinations, the patients that suffer from

breast cancer were diagnosed. After the patients had gone through radical mastectomy, both the breast tumor and para-tumor tissues and at least 10 lymph nodes were investigated pathologically after they were gathered. Below is the presentation of the related inclusion criteria. The patients possessed no serious organ dysfunction, no other malignant tumor types, full clinical data, and no bilateral breast cancer; and did not receive radiotherapy or chemotherapy prior to the surgery. The tissues were fixed in the 10% formalin and were paraffin-embedded to carry out both the histological examination and IHC. To carry out the protein expression analyses, certain tissues were snap-frozen in liquid nitrogen.

2.19. *Statistical analysis*

Data were expressed as the mean ± standard deviation (SD) from at least 3 separate experiments, and the group differences were explored through the use of the Chi-Square test, the Student's *t*-test or the Mann–Whitney U test in suitable cases. DFS and overall survival per group were assessed employing the Kaplan-Meier method and were explored by using the log-rank test. SPSS 23.0 was employed in order to carry out the statistical analyses. It is thought that the $P \leq 0.05$ was statistically significant.

3. Results and discussion

3.1. *Drug accumulates in lysosomes in drug-resistant breast cancer cells*

To investigate the correlation of drug distribution with cell resistance, low-dose of docetaxel was used to induce the drug-resistant MDA-MB-231 cells (termed as 231-DR). MDA-MB-231 cells were treated with increasing doses of docetaxel, and dosage was increased in a stepwise pattern when normal cell proliferation resumed (Fig. 1A). 231-DR cells exhibited 3.6-fold higher IC50 values compared to MDA-MB-231 Parental cell (termed as 231-PA) cells (Fig. 1B). To observe the intracellular drug distribution, fluorescently labeled drug docetaxel-488 was cocultured with cells for 2 h. Cell imaging revealed that docetaxel distributed in cytoplasm in a discrete form in the 231-PA cells (Fig. 1C). For 231-DR cells, the overlap of the fluorescence of drugs and lysosomes was confirmed, indicating the aggregation of drugs in lysosomes within drug-resistant cells. Meanwhile, transmission electron microscope results revealed that there was an increase of lysosome quantity when comparing 231-DR cells with 231-PA cells (Fig. 1D). Based on these results, we hypothesized that the increased quantity of lysosome and the drug aggregation effect of lysosome contributed to drug resistance. Similar results can also be found *in vivo*. 231-PA and 231-DR cells were inoculated into breast fat pads of female nude mice, respectively. After tumor formation, mice were treated with docetaxel three times (10 mg/kg) (Fig. 1E). 231-DR cells grew much faster than 231-PA cells without significant weight change (Fig. 1F). Meanwhile, the number of lysosomes in drug-resistant 231-DR tissues was much higher than that in 231-PA tissues, which was consistent with *in vitro* results (Figs. 1G and S1A).

3.2. *V-ATPase inhibitor could enhance the chemotherapeutic effect of breast cancer*

V-ATPase serves as a proton pump to maintain the stability of lysosome. An increase of the V-ATPase subunit ATP6V0A1 or ATP6V1B2 was confirmed in drug-resistant 231-DR mouse model through immunohistochemistry (IHC) and western blotting (WB) analysis (Fig. 1H and 1I). Then, we would like to explore the relationship between V-ATPase and drug resistance. Cells were treated with concanamycin A (CMA) or bafilomycin A1 (BAF), which are specific inhibitors of V-ATPase [6]. Inhibition of lysosomal V-ATPase successfully abrogated the lysosomal aggregation of docetaxel (Fig. 2A). Then, we evaluated the impacts of V-ATPase inhibitors alone and the combination therapy (V-ATPase inhibitors + chemical drug) on breast cancer cell growth, and confirmed that BAF or CMA could successfully inhibit the expression of ATP6V0A1 and ATP6V1B2 (Figs. 2B and S1B). The medication of V-ATPase inhibitor resulted in inhibition of cell proliferation of several breast cancer cell lines, for example, 231-WT cells had an IC50 of 348.7 nM after the treatment of V-ATPase inhibitor (Fig. 2C). Next, we tried to verify this therapeutic effect using the NOD/SCID mouse model. NOD/SCID mice were injected with 231-DR cells, and after tumor formation mice were administrated with PBS or CMA followed by the treatment of docetaxel (Fig. 2D). CMA+docetaxel group exhibited a decreased tumor volume and ATP6V0A1 expression compared to the PBS+docetaxel group (Fig. 2E and 2F). At the same time, we observed that the mice treated by CMA displayed a decreased quantity of lysosome in cytoplasm (Fig. 2G).

3.3. *KCNJ15 was associated with drug sensitivity of breast cancer cells*

V-ATPase inhibitor CMA could relieve drug resistance by changing the structure of V-ATPase. However, in view of the fact that there are two domains and fourteen protein subunits in one V-ATPase, it is difficult to regulate its function through changing just one single subunit. We hypothesized that there should be upstream regulatory proteins that could affect the V-ATPase's structure. Therefore, we sequenced the 231-PA and 231-DR cells to explore the gene expression differences; performed tandem affinity protein purification and mass spectrometry analysis (TAP-MS/MS) for identification of ATP6V0A1-interacting proteins; and analyzed a dataset of resistance and parental differential genes from GEO database (GES155478) (Fig. 3A). We intersected these three result lists and found that KCNJ15 might be the upstream regulatory protein that regulated the V-ATPase's structure. First, it was revealed that the expression of KCNJ15 was significantly lower in drug-resistant cells (Fig. S2A and S2B). Through PCR and WB experiments of paracancerous tissue and tumor tissue, KCNJ15 was significantly lower in tumor tissues (Figs. S2C and S2D). TCGA public databases also showed the lower expression of KCNJ15 in tumor tissues (Fig. S2E).

In vitro studies were conducted to further investigate the functions of KCNJ15 in breast cancer, and the expression levels of KCNJ15 were detected in several breast cancer cell lines. TNBC cells, including MDA-MB-231, MDA-MB-468 and BT549, showed much lower level of KCNJ15 than

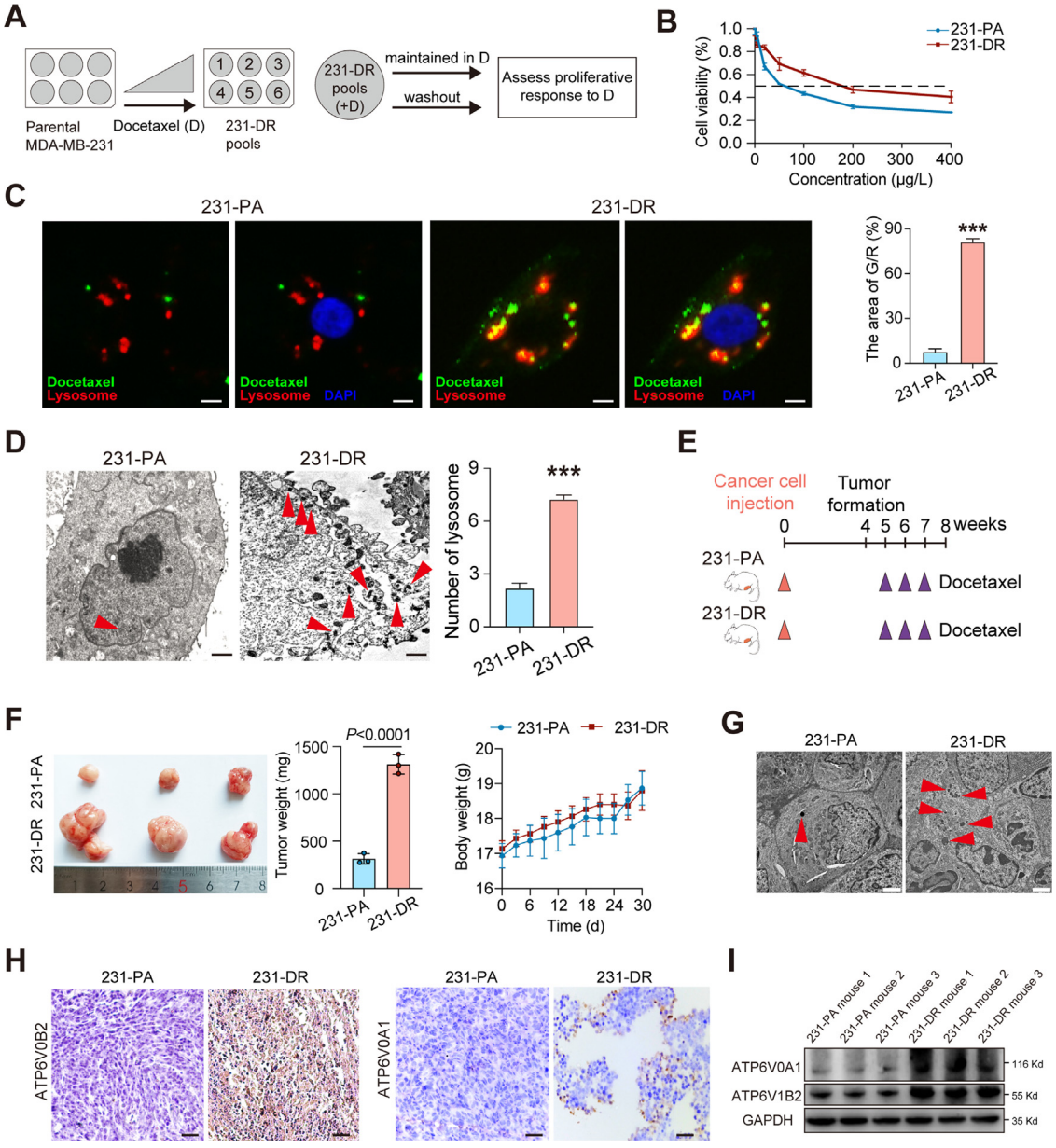

Fig. 1 – Drug accumulates in lysosomes in drug-resistant breast cancer cell. (A) process of drug resistance in 231-DR cells; (B) The drug sensitivity test of 231-DR compared to 231-PA cells. (C) The positions of the drug distributions and lysosomes in 231-DR and 231-PA cells were revealed by the fluorescence maps and statistic graphs (scale bar = 5 μm). (D) TEM images and statistic graphs of 231-DR and 231-PA cells showed that there were more lysosomes in 231-DR cells (scale bar = 2 μm). (E) The schematic diagram of the animal experimental design: the 231-PA and 231-DR cells were inoculated into female BALB/c nude mice. After tumor formation (21 d), mice were treated with docetaxel for 30 d (F) The subcutaneous tumors after the animal experiments were shown. All mice were weighed per 6 d, and the line graph represents average body weight. (G) The post-embedding electron microscopy for subcutaneous tumors (scale bar = 2 μm). (H) The embedded sections of subcutaneous tumors immunohistochemically stained for ATP6V0A1 and ATP6V02B. (I) The protein expressions of ATP6V0A1 and ATP6VB2 in subcutaneous tumors were analyzed by western blot.

normal breast cells (MCF-10A) (Fig. 3B). We then employed lentivirus to induce the stable overexpression of KCNJ15 protein in 231-PA cells (termed as OE KCNJ15 cells) (Figs. S2F–S2I). Overexpressed (OE) KCNJ15 could significantly inhibit the cell proliferation and migration (Fig. S3A–S3C), induce the apoptosis of tumor cells (Fig. S3D), and increase the cell sensitivity to drugs including docetaxel, doxorubicin, cyclophosphamide and CDK4/6 inhibitors, while knockdown of KCNJ15 showed opposite results (Fig. 3C). In addition, the number of lysosomes dramatically reduced in OE KCNJ15 (OE KCNJ15 MDA-MB-231 and OE KCNJ15 MDA-MB-468 cells (Fig. 3D). Similar results were also found at animal level.

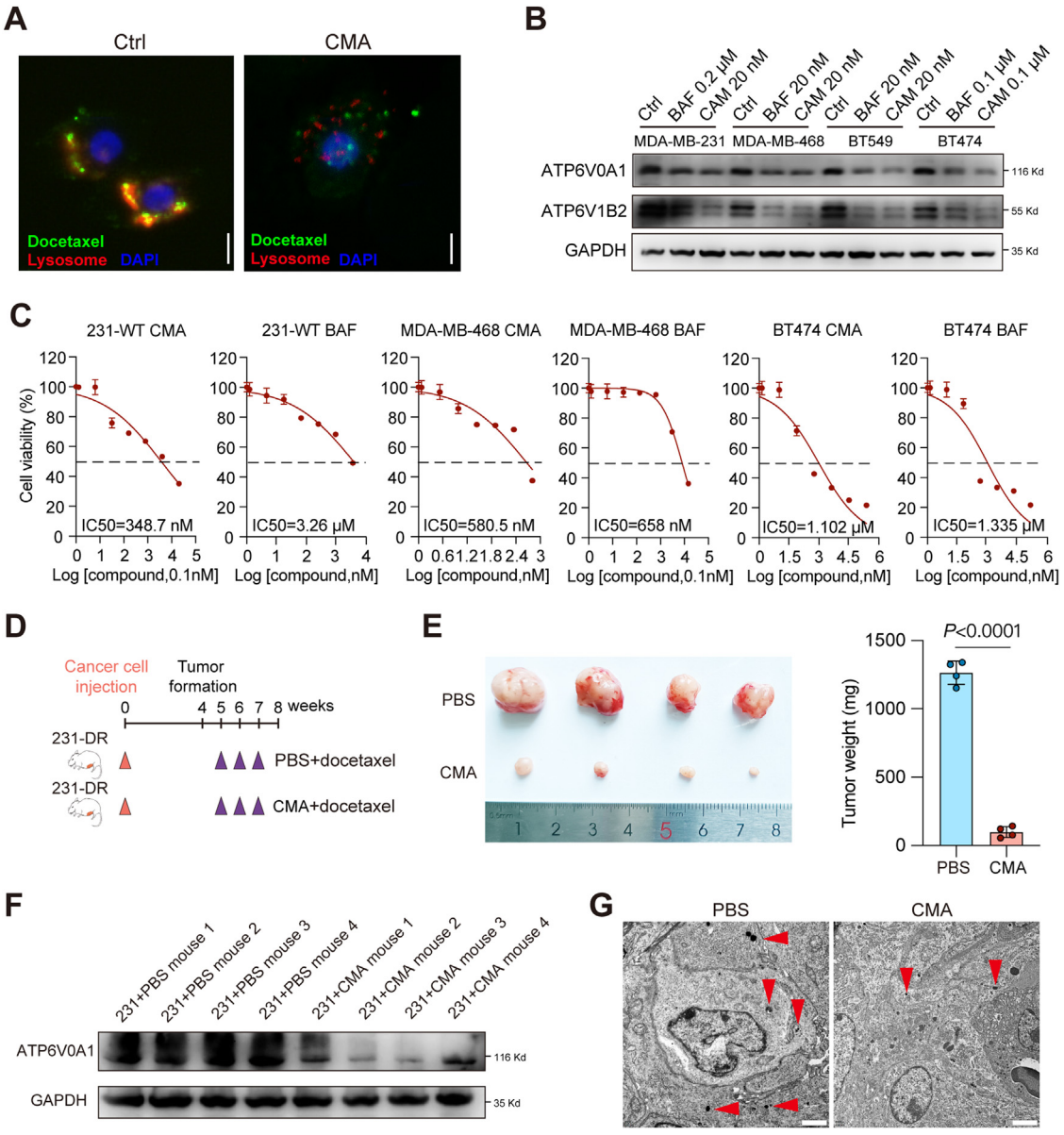

Fig. 2 – V-ATPase inhibitor could enhance the chemotherapeutic effect of breast cancer. (A) The distribution of docetaxel was changed after treatment with CAM in drug-resistant cell lines (scale bar = 5 μm). (B) After the four cell lines (MDA-MB-231, MDA-MB-468, BT549 and BT474 cells) treated with ATPase inhibitors (BAF and CAM), and the protein expressions of ATP6V0A1 and ATP6VB2 were significantly decreased by WB verification. (C) CAM and BAF inhibited the proliferation of MDA-MB-231, MDA-MB-468 and BT474 cells. (D) The schematic diagram of the animal experimental design: The 231-DR cells were inoculated into female BALB/c nude mice. After tumor formation, mice were treated with CMA or placebo. (E) The tumor was obviously reduced in the CMA treatment group. (F) The protein expressions of ATP6V0A1 in subcutaneous tumors were analyzed by western blot. (G) The post-embedding electron microscopy for subcutaneous tumors (scale bar = 2 μm).

Mice were inoculated with 231-WT, 231-NC (MDA-MB-231 with lentivirus only, the KCNJ15 expression feature was not changed), and OE KCNJ15 cells (Fig. 3E). After 4 weeks, tumors in group OE KCNJ15 were much smaller than those in the 231-WT and 231-NC groups (Fig. 3F). Through the WB experiment after extracting proteins from tumor tissues, it was found that the expression of KCNJ15 in the tumors formed by injection of OE KCNJ15 cells showed significantly high expression (Fig. 3G). Meanwhile, mice in the OE KCNJ15 group showed a longer survival than other groups without significant body weight change (Fig. 3H). These results indicated that KCNJ15 overexpression could improve the drug sensitivity of tumor cells, and inhibit the tumor growth.

3.4. *Interactions between KCNJ15 and v-ATPase*

To elucidate the molecular mechanism of KCNJ15-induced drug resistance, TAP-MS/MS was applied to identify KCNJ15-

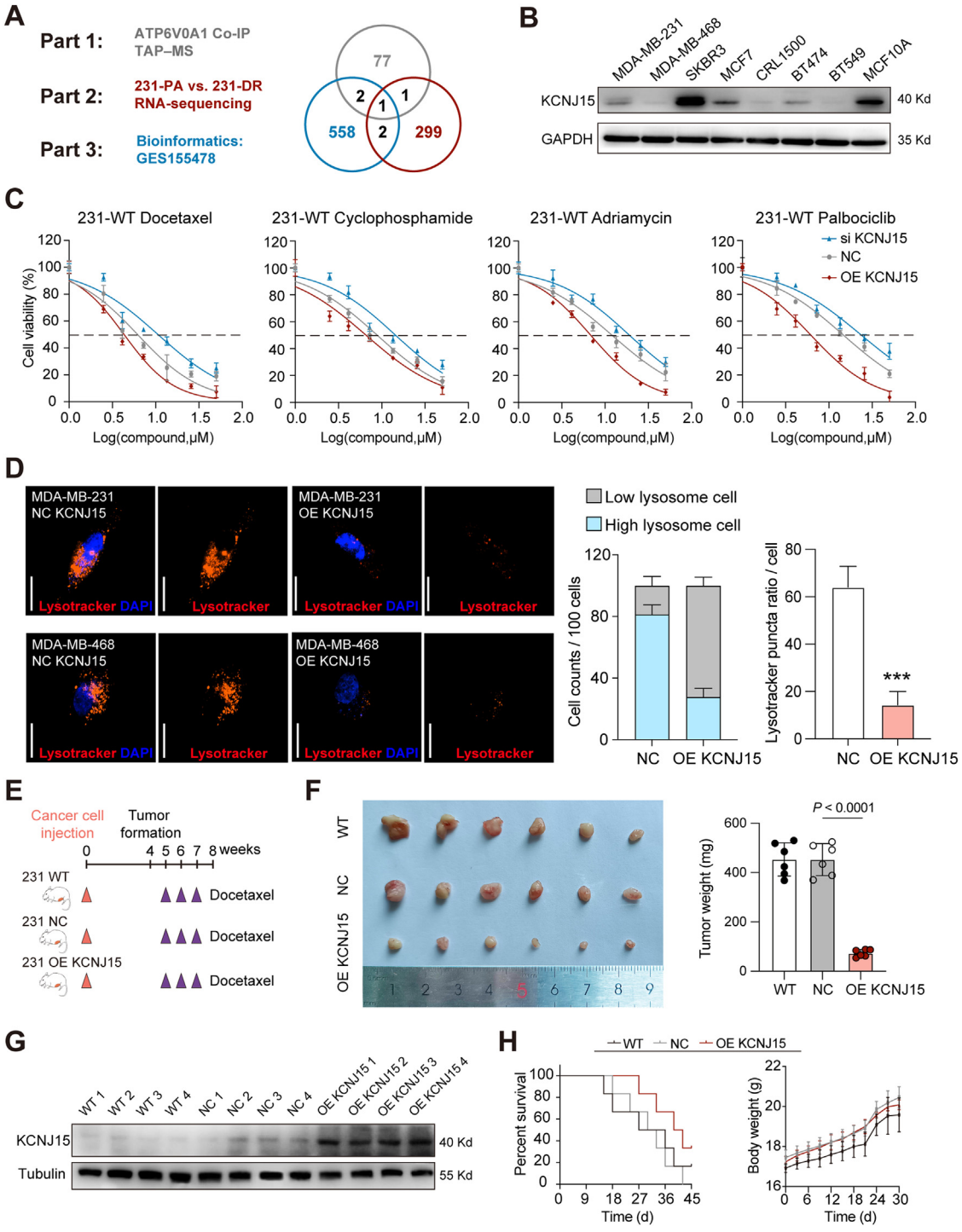

Fig. 3 – KCNJ15 is associated with drug sensitivity of breast cancer cells. (A) The schematic representation of intersection of gene expression differences between the 231-PA and 231-DR cells, ATP6V0A1-interacting proteins, and resistance and parental differential genes. (B) Comparison of KCNJ15 expression in 8 breast cancer cell lines (MCF10A were normal breast cancer cells). (C) Drug sensitivity of four commonly used chemotherapeutic drugs (docetaxel, cyclophosphamide, adriamycin, and palbociclib) in MDA-MB-231 cell lines. OE KCNJ15 could significantly increase the drug sensitivity, and knockdown of KCNJ15 inhibited the drug sensitivity. (D) OE KCNJ15 cells with stained lysosomes (scale bar = 10 μm), and the data analysis of the lysosome reduction perentage and the lysotracker change ratio in each cell. (E) The schematic diagram of the animal experimental design: The OE KCNJ15 MDA-MB-231 cells were inoculated into female BALB/c nude mice. After tumor formation (21 d), mice were treated with docetaxel for 30 d. (F) The tumor was obviously reduced in the OE KCNJ15 group. (G) The protein expressions of KCNJ15 in subcutaneous tumors were analyzed by western blot. (H) The survival curves and body weights of three groups of mice.

interacting proteins. ATP6V0A1 serves as a rotary subunit which mediates V0 coupling. ATP6V1B2 is a main part of V1 domain of v-ATPase. Our results suggested that KCNJ15 modulated v-ATPase's function through its physiological connection with ATP6V1B2 as well as ATP6V0A1 (Fig. S4). Protein structure computer simulation was applied to predict the interactions between KCNJ15 and v-ATPase. As expected, KCNJ15 was confirmed to be highly correlated with the V-ATPase subunits ATP6V0A1 and ATP6V1B2 (Fig. 4A and 4B). Co-immunoprecipitation (Co-IP) assay results demonstrated KCNJ15 binding to both ATP6V0A1 (Fig. 4C and 4D) and ATP6V1B2 (Fig. 4E and 4F). The same results can also be found in other cell lines including BT474 (Fig. 4G and S5A). ATP6V0A1 is a major regulator of V-ATPase structure, and ATP6V1B2 takes charge of V-ATPase assembly, supporting the interaction between ATP6V0A1 and ATP6V1B2 being likely to influence the V-ATPase function. Co-IP results showed that KCNJ15 could decrease the ATP6V0A1-ATP6V1B2 interaction in 231-PA cells (Fig. 4H). Conversely, KCNJ15 depletion enhanced the ATP6V0A1-ATP6V1B2 binding in 231-PA cells (Fig. 4I). Confocal results demonstrated that both endogenous and exogenous KCNJ15 were localized in cytoplasm and perinuclear regions, shown with speckled patterns in Fig. 4J. Co-fluorescence results revealed the apparent co-localization of KCNJ15 with lysosomes and ATP6V1B2 (Fig. 4K). Meanwhile, the overexpression of KCNJ15 could decrease the distribution of ATP6V1B2 (Fig. 4L).

To confirm the interaction between KCNJ15 and V-ATPase, co-IP assay of KCNJ15, ATP6V0A1, and ATP6V1B2 after the application of CAM/BAF was conducted. KCNJ15 could negatively modulate V-ATPase activity (Fig. S5B). On the other hand, we tried to inhibit the binding between KCNJ15 and v-ATPases by CMA/BAF. BAF and CMA could respectively weaken or even block the binding of KCNJ15 to ATP6V0A1 and ATP6V1B2 (Fig. 5A-5D and S5C). The results revealed that the binding between KCNJ15 and V-ATPase can be decreased by CMA/BAF. Computer simulation results indicated that there were specific interaction sites of CMA to both KCNJ15 and V-ATPase subunits ATP6V0A1/ATP6V1B2, which may inhibit the interaction between KCNJ15 and V-ATPase (Fig. 5E and 5F).

3.5. *KCNJ15 correlated with poor prognosis and drug resistance in breast cancer patients*

To explore whether our findings were clinically relevant, the correlation of the expressions of KCNJ15, ATP6V0A1, and ATP6V1B2, with patient prognosis were further investigated. Significantly low KCNJ15 expression was detected in breast cancer cells, and high expression of ATP6V0A1 and ATP6V1B2 was confirmed in 640 patient samples. There was a negative correlation between the expression score of KCNJ15 and the expressions of ATP6V0A1 and ATP6V1B2 in tumor cells (Fig. 6A and 6B). Similarly, KCNJ15 expression was inversely correlated with lysosomal quantity. Breast cancer patient tissues after neoadjuvant chemotherapy were collected and analyzed. Moreover, significantly higher expressed KCNJ15 in chemosensitive tissues in comparison to chemoresistant tissues was identified (Fig. 6C and 6D). We next evaluated the correlation of KCNJ15 expression status with the clinical and pathologic characteristics of 573 patients with invasive breast cancer. Patients with low KCNJ15 expression exhibited a relatively shorter DFS and OS than patients with high expression of KCNJ15 protein (Fig. S6A and S6B). In all subtypes of breast cancer patients who receiving chemotherapy, low KCNJ15 expression exhibited a shorter DFS (Fig. 6E). On the other hand, patients with high ATP6V0A1 expression exhibited a relatively shorter DFS and OS than patients with high expression of ATP6V0A1 protein (Fig. S7A and S7B). The present study found that KCNJ15 could weaken the assembly of V-ATPase by binding with ATP6V0A1, and the specific expression of KCNJ15 in drug-resistant TNBC was reduced, leading to the hyperfunction of lysosome, reducing the pH in lysosome, and thus mediating chemotherapy resistance (Fig. 6F). These outcomes suggested that KCNJ15 could serve as a potential indicator to predict breast cancer drug resistance, therapeutic efficacy, and overall survival before chemotherapy, providing clues for the choice of more efficacious therapeutic strategies.

3.6. *Discussion*

Drug resistance severely dampens the life expectancy of breast cancer patients. In the clinical practice, one chemotherapeutic regimen will be replaced by another one with different mechanisms of action when drug resistance occurs. Unfortunately, these patients showed poor DFS even if they received multiple lines of treatment. Moreover, sides effects induced by multiple drug treatment may lower the life quality of patients. Merging evidences show that patients have a relatively longer survival time should they be sensitive to neoadjuvant chemotherapy or other first-line treatments. Consequently, it is of vital importance to confirm the high efficiency of regimen that patients receive for the first time. In addition to the precise selection of treatment strategies, regulating and reversing drug resistance are crucial directions to obtain satisfying clinical therapeutic effects.

KCNJ15 encodes the inwardly rectifying potassium channel Kir4.2 [21], which is thought to promote migratory and metastasis of tumor cells in the tumor micro-environment [24,25]. Although prior findings have shown that KCNJ15 gene functions at malignant neoplasms, the association of KCNJ15 with malignancies remains unclear. Nakamura et al. indicated KCNJ15 an underlying oncogene in esophageal cancer progression [23]. Conversely, Liu et al. provided a proof to the contrary that KCNJ15 suppressed tumor development in renal cell carcinoma [26]. In this study, for the first time, we provided compelling evidences that KCNJ15 protein can alter the function of lysosomes *in vitro* as well as *in vivo*. Lysosome dysfunction has been revealed a major cause for drug resistance in tumor cells. Hence, the delineation of the potential mechanisms may provide possible solutions to delay the resistance-induced tumor progression. Chemotherapy resistant 231-DR breast cancer cell was sorted and collected to explore the phenotypic features. We observed that (1) the number of lysosomes in drug-resistant cells is higher than that in the drug-sensitive cells; (2) drug aggregation may occur in lysosomes, preventing them from reaching their intracellular targets and thereby inducing drug resistance. Our data provide essential proof of concept that KCNJ15 is

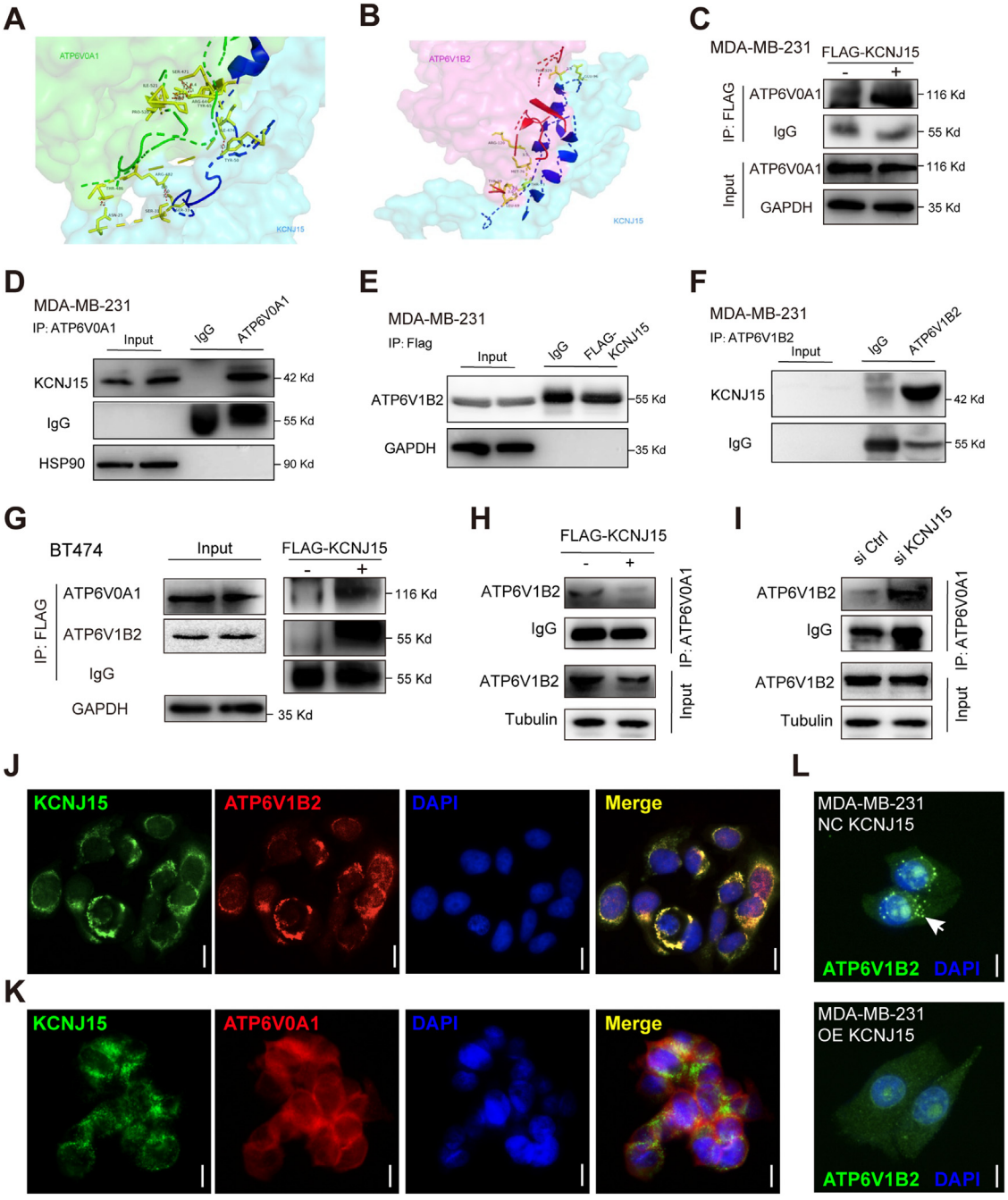

Fig. 4 – The binding of KCNJ15 to ATP6V0A1 leads to the hydrolysis of v-ATPase. (A) The structural simulation of KCNJ15 and ATP6V0A1. (B) The structural simulation of KCNJ15 and ATP6V1B2. (C) After MDA-MB-231 cells transfected with KCNJ15 plasmid, Co-IP assay was performed, and the protein expression of ATP6V0A1 was detected. (D) Co-IP assay was performed using ATP6V0A1 antibody, and the protein expression of KCNJ15 was detected. (E) After MDA-MB-231 cells transfected with KCNJ15 plasmid, Co-IP assay was performed, and the protein expression of ATP6V1B2 was detected. (F) Co-IP assay was performed using ATP6V1B2 antibody, and the protein expression of KCNJ15 was detected. (G) After BT474 cells transfected with KCNJ15 plasmid, Co-IP assay was performed, and the protein expressions of ATP6V0A1 and ATP6V1B2 were detected. (H) After KCNJ15 plasmid transfection, the combination of ATP6V0A1 and ATP6V1B2 was detected. (I) After si-KCNJ15 transfection, the combination of ATP6V0A1 and ATP6V1B2 was detected. (J) The co-localization plot of KCNJ15 and ATP6V0A1 (scale bar = 10 μm). (K) The co-localization plot of KCNJ15 and ATP6V1B2 (scale bar = 10 μm). (L) The overexpression of KCNJ15 could decrease the intracellular lysosome quantity (scale bar = 10 μm). (M) The overexpression of KCNJ15 could decrease the distribution of ATP6V1B2 (scale bar = 8 μm).

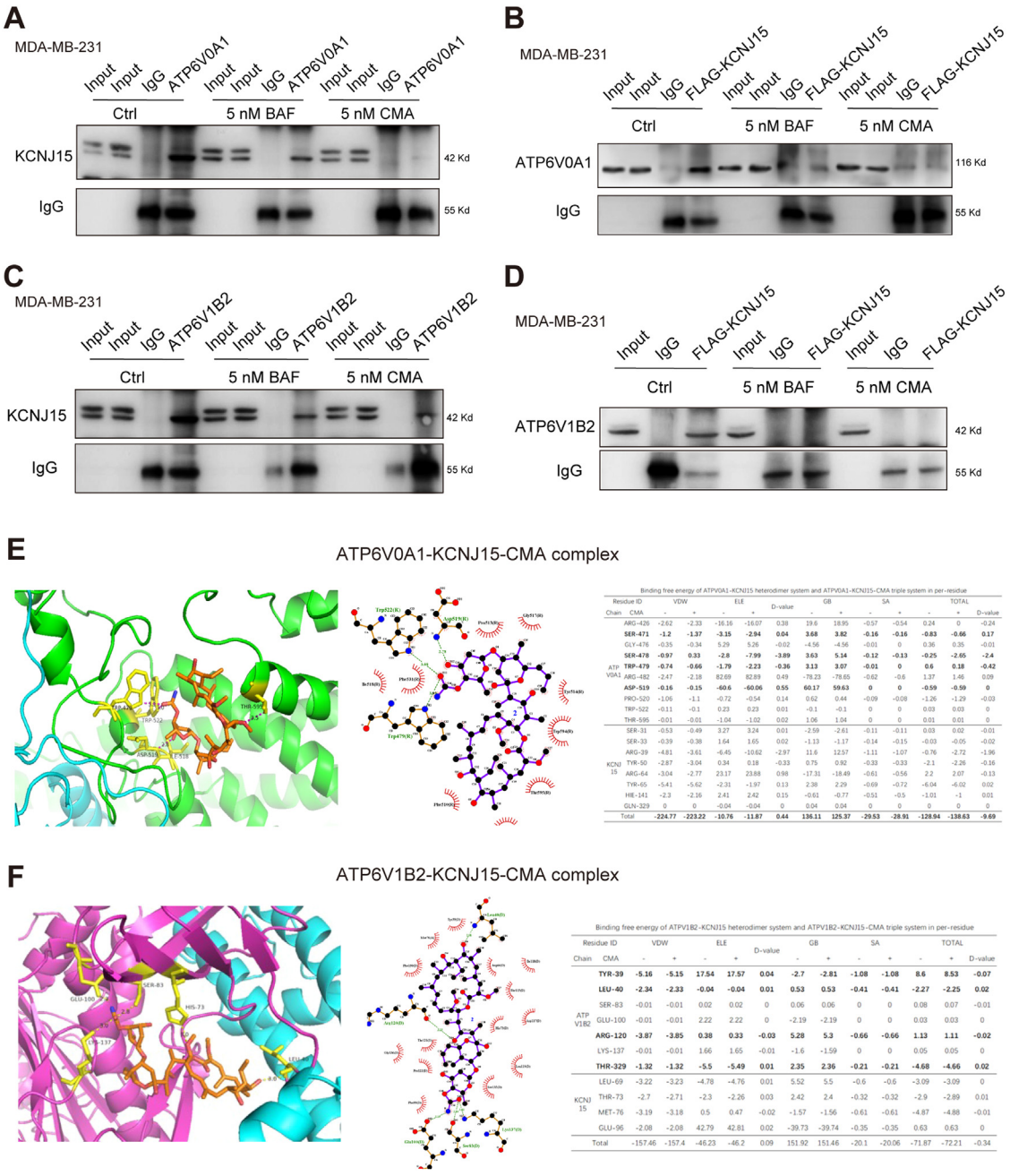

Binding free energy of ATPV0A1-KCNJ15 heterodimer system and ATPV0A1-KCNJ15-CMA triple system in per-residue

Residue ID		VDW		ELE		D-value	GB		SA		TOTAL		
Chain	CMA	-	+	-	+		-	+	-	+	-	+	D-value
ATP V0A1	ARG-426	-2.62	-2.33	-16.16	-16.07	0.38	19.6	18.95	-0.57	-0.54	0.24	0	-0.24
	SER-471	**-1.2**	**-1.37**	**-3.15**	**-2.94**	**0.04**	**3.68**	**3.82**	**-0.16**	**-0.16**	**-0.83**	**-0.66**	**0.17**
	GLY-476	-0.35	-0.34	5.29	5.26	-0.02	-4.56	-4.56	-0.01	0	0.36	0.35	-0.01
	SER-478	**-0.97**	**0.33**	**-2.8**	**-7.99**	**-3.89**	**3.63**	**5.14**	**-0.12**	**-0.13**	**-0.25**	**-2.65**	**-2.4**
	TRP-479	**-0.74**	**-0.66**	**-1.79**	**-2.23**	**-0.36**	**3.13**	**3.07**	**-0.01**	**0**	**0.6**	**0.18**	**-0.42**
	ARG-482	-2.47	-2.18	82.69	82.89	0.49	-78.23	-78.65	-0.62	-0.6	1.37	1.46	0.09
	ASP-519	**-0.16**	**-0.15**	**-60.6**	**-60.06**	**0.55**	**60.17**	**59.63**	**0**	**0**	**-0.59**	**-0.59**	**0**
	PRO-520	-1.06	-1.1	-0.72	-0.54	0.14	0.62	0.44	-0.09	-0.08	-1.26	-1.29	-0.03
	TRP-522	-0.11	-0.1	0.23	0.23	0.01	-0.1	-0.1	0	0	0.03	0.03	0
	THR-595	-0.01	-0.01	-1.04	-1.02	0.02	1.06	1.04	0	0	0.01	0.01	0
KCNJ 15	SER-31	-0.53	-0.49	3.27	3.24	0.01	-2.59	-2.61	-0.11	-0.11	0.03	0.02	-0.01
	SER-33	-0.39	-0.38	1.64	1.65	0.02	-1.13	-1.17	-0.14	-0.15	-0.03	-0.05	-0.02
	ARG-39	-4.81	-3.61	-6.45	-10.62	-2.97	11.6	12.57	-1.11	-1.07	-0.76	-2.72	-1.96
	TYR-50	-2.87	-3.04	0.34	0.18	-0.33	0.75	0.92	-0.33	-0.33	-2.1	-2.26	-0.16
	ARG-64	-3.04	-2.77	23.17	23.88	0.98	-17.31	-18.49	-0.61	-0.56	2.2	2.07	-0.13
	TYR-65	-5.41	-5.62	-2.31	-1.97	0.13	2.38	2.29	-0.69	-0.72	-6.04	-6.02	0.02
	HIE-141	-2.3	-2.16	2.41	2.42	0.15	-0.61	-0.77	-0.51	-0.5	-1.01	-1	0.01
	GLN-329	0	0	-0.04	-0.04	0	0.04	0.04	0	0	0	0	0
	Total	**-224.77**	**-223.22**	**-10.76**	**-11.87**	**0.44**	**136.11**	**125.37**	**-29.53**	**-28.91**	**-128.94**	**-138.63**	**-9.69**

Binding free energy of ATPV1B2-KCNJ15 heterodimer system and ATPV1B2-KCNJ15-CMA triple system in per-residue

Residue ID		VDW		ELE		D-value	GB		SA		TOTAL		
Chain	CMA	-	+	-	+		-	+	-	+	-	+	D-value
ATP V1B2	**TYR-39**	**-5.16**	**-5.15**	**17.54**	**17.57**	**0.04**	**-2.7**	**-2.81**	**-1.08**	**-1.08**	**8.6**	**8.53**	**-0.07**
	LEU-40	**-2.34**	**-2.33**	**-0.04**	**-0.04**	**0.01**	**0.53**	**0.53**	**-0.41**	**-0.41**	**-2.27**	**-2.25**	**0.02**
	SER-83	-0.01	-0.01	0.02	0.02	0	0.06	0.06	0	0	0.08	0.07	-0.01
	GLU-100	-0.01	-0.01	2.22	2.22	0	-2.19	-2.19	0	0	0.03	0.03	0
	ARG-120	**-3.87**	**-3.85**	**0.38**	**0.33**	**-0.03**	**5.28**	**5.3**	**-0.66**	**-0.66**	**1.13**	**1.11**	**-0.02**
	LYS-137	-0.01	-0.01	1.66	1.65	-0.01	-1.6	-1.59	0	0	0.05	0.05	0
	THR-329	**-1.32**	**-1.32**	**-5.5**	**-5.49**	**0.01**	**2.35**	**2.36**	**-0.21**	**-0.21**	**-4.68**	**-4.66**	**0.02**
KCNJ 15	LEU-69	-3.22	-3.23	-4.78	-4.76	0.01	5.52	5.5	-0.6	-0.6	-3.09	-3.09	0
	THR-73	-2.7	-2.71	-2.3	-2.26	0.03	2.42	2.4	-0.32	-0.32	-2.9	-2.89	0.01
	MET-76	-3.19	-3.18	0.5	0.47	-0.02	-1.57	-1.56	-0.61	-0.61	-4.87	-4.88	-0.01
	GLU-96	-2.08	-2.08	42.79	42.81	0.02	-39.73	-39.74	-0.35	-0.35	0.63	0.63	0
	Total	-157.46	-157.4	-46.23	-46.2	0.09	151.92	151.46	-20.1	-20.06	-71.87	-72.21	-0.34

Fig. 5 – V-ATPase inhibitor could block the binding of KCNJ15 to ATP6V0A1. (A) Co-IP assay was performed using ATP6V0A1 antibody in MDA-MB-231 cells (BAF, CMA and control groups), and the protein expression of KCNJ15 was detected. The combination was weakened in BAF and CMA groups. (B) Co-IP assay was performed in MDA-MB-231 cells transfected with KCNJ15 plasmid (BAF, CMA and control groups), and the protein expression of ATP6V0A1 was detected. The combination was weakened in BAF and CMA groups. (C) Co-IP assay was performed using ATP6V1B2 antibody in MDA-MB-231 cells (BAF, CMA and control groups), and the protein expression of KCNJ15 was detected. (D) Co-IP assay was performed in MDA-MB-231 cells transfected with KCNJ15 plasmid (BAF, CMA and control groups), and the protein expression of ATP6V1B2 was detected. The combination was weakened in BAF and CMA groups. (E) The structural simulation of CMA blocking the binding of KCNJ15 to ATP6V0A1. (F) The structural simulation of CMA blocking the binding of KCNJ15 to ATP6V1B2.

an important protein to maintain the stability of lysosomes (Fig. 6F).

V-ATPase, consisting of several subunits, exerts vital effects on determining the lysosomal steady-state pH, with an ATP-dependent process of pumping protons into lysosomal lumens [14,27,28]. It was revealed that the intracellular KCNJ15 protein can bind to ATP6V0A1, thus facilitating separation of V0 and V1 subunits in V-ATPase and inhibiting proton pump effects of V-ATPase. In addition, we established that a small molecule drug CMA/BAF can reverse drug

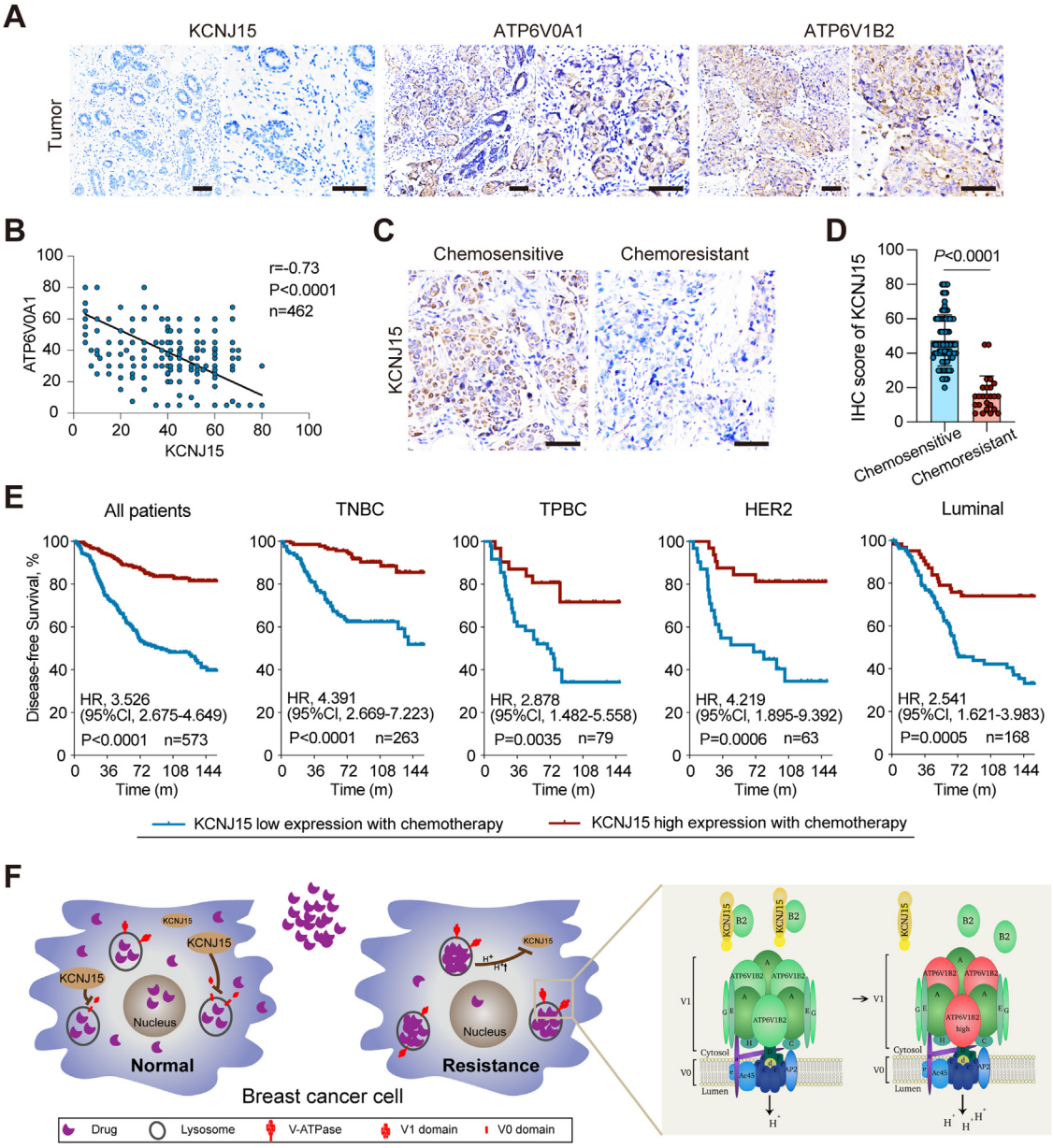

Fig. 6 – KCNJ15 is associated with poor prognosis and drug resistance in patients with breast cancer. (A) Tissues from patients with TNBC were processed for IHC and stained with the antibodies of KCNJ15, ATP6V0A1 and ATP6V1B2, and the representative graphs were presented (scale bar = 50 μm). (B) The correlation analysis between the IHC scores of KCNJ15 and ATP6V0A1 showed that a negative correlation with R equal to −0.73. (C) The typical diagrams of neoadjuvant efficacy grouping (chemosensitive *vs* chemoresistant) (scale bar = 50 μm). (Dd) The IHC scores of KCNJ15 in the chemosensitive and chemoresistant groups. (E) All patients (treated with chemotherapy) and patients with 4 types (TNBC, TPBC, HER2 and luminal) were divided into two groups according to the IHC scores of KCNJ15, respectively. The survival chart showed their differences in DFS. (F) The pattern graph of this study. KCNJ15 could weaken the assembly of V-ATPase by binding with ATP6V0A1, and the reduced expression of KCNJ15 in drug-resistant triple negative breast cancer led to the hyperfunction of lysosome, the reduction of PH in lysosome, and the modification of chemotherapy resistance.

resistance by disrupting the interaction between KCNJ15 and lysosomes. Noteworthy, CMA/BAF, which belongs to the plecomacrolide class, usually functions as an antibiotic [29]. Although CMA/BAF was traditionally used to suppress the invasiveness of breast cancer cells through its inhibitory effects on V-ATPase, few studies have shown the clinical value of CMA/BAF for drug-resistant breast cancer treatment [30,31]. In this study, for the first time, we established that CMA/BAF could enhance sensitivity of breast cancer cells to chemotherapy drugs, target drugs, and CDK4/6 inhibitors *in vitro*. Moreover, we revealed that CMA/BAF could inhibit tumor growth and prolong the survival time *in vivo*, highlighting its

potential for therapeutic strategies of drug-resistant breast cancer.

To explore the clinical significance of KCNJ15, tumor tissues after neoadjuvant were collected and analyzed. Patients who were drug resistant showed lower expression of KCNJ15 protein compared with those who were drug sensitive. Moreover, in more than 10 years follow-up peroid, we found that DFS was relatively shorter in KCNJ15 low-expression patients compared to KCNJ15 high-expression patients. In conclusion, our findings suggested that KCNJ15 could serve as a potential indicator to predict breast cancer drug resistance, therapeutic efficacy, and overall survival before chemotherapy. Therefore, our work may provide a guideline for choosing appropriate treatment regimen.

4. Conclusion

The study found that KCNJ15 had low specific expression in triple-negative breast cancer, especially in paclitaxel-resistant triple-negative breast cancer cells, and clarified the regulatory effect of KCNJ15 on triple-negative breast cancer. It was found that KCNJ15 could regulate the assembly of V-ATPase by binding to ATP6V0A1, thereby affecting the mechanism of lysosomal acidity-mediated drug resistance. Based on blocking the binding plane of KCNJ15 and ATP6V0A1, it was found that the V-ATPase inhibitor CMA could effectively reverse chemotherapy resistance, which provided a new therapeutic target and opened a new path for the treatment of triple-negative breast cancer.

Conflicts of interest

The authors declare no conflict of interest.

Acknowledgments

Xinbo Qiao, Yixiao Zhang, and Zhan Zhang contributed equally to this work. This work was supported by the National Natural Science Foundation of China (#81872159, #81902607, and #81874301), the Liaoning Colleges Innovative Talent Support Program (#Cancer Stem Cell Origin and Biology Behavior), the Major Project Construction Foundation of China Medical University (#2017ZDZX05), the Outstanding Scientific Fund of Shengjing Hospital (#201803), and the Outstanding Young Scholars of Liaoning Province (#2019-YQ-10).

Supplementary materials

Supplementary material associated with this article can be found, in the online version, at doi:10.1016/j.ajps.2023.100814.

References

[1] Nussinov R, Tsai CJ, Jang H. Anticancer drug resistance: an update and perspective. Drug. Resist Updat 2021;59:100796.
[2] Lim ZF, Ma PC. Emerging insights of tumor heterogeneity and drug resistance mechanisms. in lung cancer targeted therapy. J Hematol Oncol 2019;12:134.
[3] Bugter JM, Fenderico N, Maurice MM. Mutations and mechanisms of WNT pathway. tumour suppressors in cancer. Nat Rev Cancer 2021;21:5–21.
[4] Nayar U, Cohen O, Kapstad C, Cuoco MS, Waks AG, Wander SA, et al. Acquired HER2. mutations in ER(+) metastatic breast cancer confer resistance to estrogen receptor-directed therapies. Nat Genet 2019;51 207-16.
[5] Qin S, Jiang J, Lu Y, Nice EC, Huang C, Zhang J, et al. Emerging role of tumor cell plasticity. in modifying therapeutic response. Signal Transduct Target Ther 2020;5: 228.
[6] Hangauer MJ, Viswanathan VS, Ryan MJ, Bole D, Eaton JK, Matov A, et al. Drug-tolerant. persister cancer cells are vulnerable to GPX4 inhibition. Nature 2017;551 247-50.
[7] Smith MP, Brunton H, Rowling EJ, Ferguson J, Arozarena I, Miskolczi Z, et al. Inhibiting. drivers of non-mutational drug tolerance is a salvage strategy for targeted melanoma therapy. Cancer Cell 2016;29 270-84.
[8] Comoglio PM, Trusolino L, Boccaccio C. Known and novel roles of the MET oncogene in. cancer: a coherent approach to targeted therapy. Nat Rev Cancer 2018;18 341-58.
[9] Mullard A. Addressing cancer's grand challenges. Nat Rev Drug Discov 2020;19 825-6.
[10] Sharma P, Hu-Lieskovan S, Wargo JA, Ribas A. Primary, adaptive, and acquired. resistance to cancer immunotherapy. Cell 2017;168 707-23.
[11] Ballabio A, Bonifacino JS. Lysosomes as dynamic regulators of cell and organismal. homeostasis. Nat Rev Mol Cell Biol 2020;21 101-18.
[12] Lawrence RE, Zoncu R. The lysosome as a cellular centre for signalling, metabolism and. quality control. Nat Cell Biol 2019;21 133-42.
[13] Zhang Z, Yue P, Lu T, Wang Y, Wei Y, Wei X. Role of lysosomes in physiological. activities, diseases, and therapy. J Hematol Oncol 2021;14:79.
[14] Abu-Remaileh M, Wyant GA, Kim C, Laqtom NN, Abbasi M, Chan SH, et al. Lysosomal. metabolomics reveals V-ATPase- and mTOR-dependent regulation of amino acid efflux from lysosomes. Science 2017;358 807-13.
[15] Wang L, Wu D, Robinson CV, Wu H, Fu TM. Structures of a complete kuman V-ATPase. reveal mechanisms of its assembly. Mol Cell 2020;80 501-11 e503.
[16] Santos-Pereira C, Rodrigues LR, Corte-Real M. Emerging insights on the role of V-ATPase in human diseases: therapeutic challenges and opportunities. Med Res Rev 2021;41 1927-64.
[17] Vasanthakumar T, Rubinstein JL. Structure and roles of V-type ATPases. Trends Biochem Sci 2020;45:295–307.
[18] Ramirez C, Hauser AD, Vucic EA. Bar-Sagi D. Plasma membrane V-ATPase controls. oncogenic RAS-induced macropinocytosis. Nature 2019;576 477-81.
[19] Stransky L, Cotter K, Forgac M. The function of V-ATPases in cancer. Physiol Rev 2016;96 1071-91.
[20] Jung YS, Stratton SA, Lee SH, Kim MJ, Jun S, Zhang J, et al. TMEM9-v-ATPase activates. Wnt/beta-Catenin signaling Via APC lysosomal degradation for liver regeneration and tumorigenesis. Hepatology 2021;73 776-94.
[21] Nakajima KI, Zhu K, Sun YH, Hegyi B, Zeng Q, Murphy CJ, et al. KCNJ15/Kir4.2 couples. with polyamines to sense weak extracellular electric fields in galvanotaxis. Nat Commun 2015;6:8532.
[22] Bignon Y, Pinelli L, Frachon N, Lahuna O, Figueres L, Houillier P, et al. Defective. bicarbonate reabsorption in Kir4.2 potassium channel deficient mice impairs acid-base balance and ammonia excretion. Kidney Int 2020;97:304–15.

[23] Nakamura S, Kanda M, Koike M, Shimizu D, Umeda S, Hattori N, et al. KCNJ15. Expression and malignant behavior of esophageal squamous cell carcinoma. Ann Surg Oncol 2020;27 2559-68.
[24] Veeravalli KK, Ponnala S, Chetty C, Tsung AJ, Gujrati M, Rao JS. Integrin alpha9beta1-mediated cell migration in glioblastoma via SSAT and Kir4.2 potassium channel pathway. Cell Signal 2012;24 272-81.
[25] deHart GW, Jin T, McCloskey DE, Pegg AE, Sheppard D. The alpha9beta1 integrin. enhances cell migration by polyamine-mediated modulation of an inward-rectifier potassium channel. Proc Natl Acad Sci U S A 2008;105 7188-93.
[26] Liu Y, Wang H, Ni B, Zhang J, Li S, Huang Y, et al. Loss of KCNJ15 expression promotes. malignant phenotypes and correlates with poor prognosis in renal carcinoma. Cancer Manag Res 2019;11 1211-20.
[27] Mindell JA. Lysosomal acidification mechanisms. Annu Rev Physiol 2012;74:69–86.
[28] Colacurcio DJ, Nixon RA. Disorders of lysosomal acidification-The emerging role of v-ATPase in aging and neurodegenerative disease. Ageing Res Rev 2016;32:75–88.
[29] Painter MM, Zimmerman GE, Merlino MS, Robertson AW, Terry VH, Ren X, et al. Concanamycin A counteracts HIV-1 Nef to enhance immune clearance of infected primary cells by cytotoxic T lymphocytes. Proc Natl Acad Sci U S A 2020;117 23835-46.
[30] Morais-Santos F, Miranda-Goncalves V, Pinheiro S, Vieira AF, Paredes J, Schmitt FC, et al. Differential sensitivities to lactate transport inhibitors of breast cancer cell lines. Endocr Relat Cancer 2014;21:27–38.
[31] Tavares-Valente D, Sousa B, Schmitt F, Baltazar F, Queiros O. Disruption of pH. dynamics suppresses proliferation and potentiates doxorubicin cytotoxicity in breast cancer cells. Pharmaceutics 2021;13.